A Unified Approach to Nonlinear Buckling Optimization of Composite Structures

Lindgaard, Esben; Lund, Erik

A Unified Approach to Nonlinear Buckling Optimization of Composite Structures

Esben Lindgaard*, Erik Lund*

Department of Mechanical Engineering, Aalborg University, Pontoppidanstraede 101, DK-9220 Aalborg East, Denmark

Abstract

A unified approach to nonlinear buckling fiber angle optimization of laminated composite shell structures is presented. The method includes loss of stability due to bifurcation and limiting behaviour. The optimization formulation is formulated as a mathematical programming problem and solved using gradient-based techniques. Buckling of a well-known cylindrical shell benchmark problem is studied and the solutions found in literature are proved to be incorrect. The nonlinear buckling optimization formulation is benchmarked against the traditional linear buckling optimization formulation through several numerical optimization cases of a composite cylindrical shell panel which clearly illustrates the advantage and potential of the presented approach.

Keywords: Composite laminate optimization, Nonlinear buckling, Design sensitivity analysis, Composite structures, Limit point buckling, Bifurcation buckling

1. Introduction

The use of fibre-reinforced polymers has gained an ever-increasing popularity due to their superior mechanical properties. Designing structures made out of composite material represents a challenging task, since both thicknesses, number of plies in the laminate and their relative orientation must be selected. The best use of the capabilities of the material can only be gained through a careful selection of the layup. This work focuses on optimal design of laminated composite shell structures i.e. the optimal fiber orientations within the laminate which is a complicated problem. One of the most significant advances of optimal design of laminate composites is the ability of tailoring the material to meet particular structural requirements with little waste of material capability. Perfect tailoring of a composite material yields only the stiffness and strength required in each direction. A survey of optimal design of laminated plates and shells can be found in [1].

Stability is one of the most important objectives/constraints in structural optimization and this also holds for many laminated composite structures, e.g. a wind turbine blade. Traditionally, stability is regarded as the linear buckling

---

load, but for structures exhibiting a nonlinear response when loaded, and especially for shell like structures, the traditional approach can lead to unreliable predictions of the buckling load. In the case where nonlinear effects cannot be ignored nonlinear path tracing analysis is necessary. For limit point instability, several standard finite element procedures allow the nonlinear equilibrium path to be traced until a point just before the limit point. The traditional Newton like methods will probably fail in the vicinity of the limit point and the post-critical path cannot be traced. More sophisticated techniques, as the arc-length methods suggested by [2] and subsequently modified by [3] and [4] are among some of the techniques available today for path tracing analysis in the post-buckling regime. Despite such sophisticated techniques exist, buckling analysis of shell like structures is today still a difficult task which consequently makes it difficult to optimize shell structure w.r.t. stability.

For many years a common shell buckling problem, first introduced by [5] and later appeared in numerous journal articles, has been a classical example for describing buckling behaviour of cylindrical shell panels. The example has been used as a benchmark to investigate advances in numerical finite elements methods for handling load and/or deflection reversals in nonlinear buckling problems. Furthermore, it is used to demonstrate the capability of finite element procedures to traverse such complicated load paths.

Lately, [6, 7] noticed that the solution by [5] and re-produced by many other authors through several decades was incorrect. The incorrect solution only involves symmetric deformation modes and makes the assumption that limit point buckling occurs. [6, 7] discovered through numerical studies and related experiments that the former symmetric solution is incorrect and the existence of bifurcation and asymmetric buckling mode at a lower load level. Furthermore, [6, 7] concludes that the bifurcation point is stable which means that the structure is able to carry more load after bifurcation until, according to [6, 7], a load limit point instability is encountered. The results by [6, 7] is also included and discussed in the book by [8]. Their conclusion about stability of the bifurcation point turns out to be incorrect, i.e. the bifurcation point is not stable but unstable, which demonstrates that buckling analysis of relatively simple structures still represent a challenging task. The entire solution of the buckling benchmark problem is shown in Section 4 where new features of the buckling problem are revealed.

Research on the subject of structural optimization of composite structures considering stability has been reported by many investigators. The first work to appear concerned simple composite laminated plates and circular cylindrical shells where stability was determined by solution of buckling differential equations, see [9, 10, 11, 12, 13, 14, 15, 16, 17, 18]. Later, buckling optimization of composite structures was considered in a finite element framework where the buckling load was determined by the solution to the linearized discretized matrix eigenvalue problem at an initial prebuckling point. Optimization of laminated composite plates has been studied by [19, 20, 21, 22, 23], while others considered more complex composite structures as curved shell panels and circular cylindrical shells, see [24, 25, 26, 27, 28, 29]. Applications of optimization methods to stability analysis including nonlinear prebuckling effects have been very limited. To the best knowledge of the authors only the papers by [30, 31, 32] report on nonlinear gradient based buckling optimization of composite laminated plates and shells where buckling is considered in terms of the limit load of the structure. Thus there is a lack of optimization procedures that handles bifurcation instability

2

including nonlinear prebuckling effects but also optimization procedures that simultaneously handles bifurcation and limit point instability. Despite bifurcation points, if unstable, in many cases may be transformed into limit points by introducing imperfections into the system, see e.g. [33, 34, 35], whereby only limit points may be concerned in the optimization formulation in order to optimize the buckling load, a general optimization formulation that handles both types of instability may prove to be important. In cases of stable bifurcation points the method of introducing imperfections will not work since the stability point simply vanish, i.e. the bifurcation point is not converted into a limit point but vanish and the load response keeps rising stably. Also in cases of unstable bifurcation points the method of introducing imperfections may not be without difficulties since a proper choice of imperfections can be difficult. The latter is shown in Section 4. Furthermore, the type of stability may also change during buckling optimization, i.e. from one optimization iteration to another the stability type may change from e.g. a bifurcation point to a limit point. An optimization formulation that operates on the initial structure without imperfections and handles a general type of stability is needed.

This paper presents an integrated and reliable method for doing optimization of composite structures w.r.t. a general type stability, i.e. bifurcation instability and limit point instability, depending on what to appear first on the equilibrium path. Features for detecting bifurcation points and limit points during nonlinear path tracing analysis is developed. The nonlinear buckling formulation described in [31] is utilized, i.e. optimization w.r.t. stability is accomplished by including the nonlinear response by a path tracing analysis, after the arc-length method, in the optimization formulation, using the Total Lagrangian formulation. The nonlinear path tracing analysis is stopped when a stability point is encountered and the critical load is approximated at a precritical load step according to the "one-point" approach, i.e. the stiffness information is extrapolated from one precritical equilibrium point until a singular tangent stiffness is obtained. Design sensitivities of the critical load factor are obtained semi-analytically by the direct differentiation approach on the approximate eigenvalue problem described by discretized finite element matrix equations. A number of the lowest buckling load factors are considered in the optimization formulation in order to avoid problems related to "mode switching". The proposed method is benchmarked against a formulation based on linear buckling analysis on a shell buckling problem and helps to clarify the importance of including nonlinear prebuckling effects in structural design optimization w.r.t. stability.

In this work only Continuous Fiber Angle Optimization (CFAO) is considered, thus fiber orientations in laminate layers with preselected thickness and material are chosen as design variables in the laminate optimization. Despite fiber angle optimization is known to be associated with a non-convex design space with many local minima it has been applied since the laminate parametrization has not been the focus in this work, i.e. the presented method in this paper is generic and can easily be used with other parametrizations.

The proposed procedure regarding nonlinear buckling analysis is described in Section 2 together with detection features applied for discovering stability points during geometrically nonlinear analysis. Derivations of design sensitivities, using the direct approach, of the nonlinear buckling load are presented along with the general type nonlinear buckling optimization formulation in Section 3. The benchmark shell buckling problem is treated in Section 4 where it

is shown that the solutions found in literature still are not correct and new features of the problem are revealed. Buckling optimization of a composite laminated curved shell panel is considered in Section 5. Conclusions are outlined in Section 6.

2. Nonlinear Buckling Analysis of Composite Structures

The finite element method is used for determining the nonlinear buckling load factor of the laminated composite structure, thus the derivations are given in a finite element context.

A laminated composite is typically composed of multiple materials and multiple layers, and the shell structures can in general be curved or doubly-curved. The materials used in this work are fiber reinforced polymers, e.g. Glass or Carbon Fiber Reinforced Polymers (GFRP/CFRP), oriented at a given angle θ_k for the kth layer. All materials are assumed to behave linearly elastic and the structural behaviour of the laminate is described using an equivalent single layer theory where the layers are assumed to be perfectly bonded together such that displacements and strains will be continuous across the thickness.

The solid shell elements used are derived using a continuum mechanics approach so the laminate is modelled with a geometric thickness in three dimensions, see [36]. The element used is an eight node isoparametric element where shear locking and trapezoidal locking is avoided by using the concepts of assumed natural strains for respectively out of plane shear interpolation, see [37], and through the thickness interpolation, see [38]. Membrane and thickness locking is avoided by using the concepts of enhanced assumed strain for the interpolation of the membrane and thickness strains respectively, see [39].

2.1. Nonlinear buckling analysis

Structural stability/buckling is estimated in terms of geometrically nonlinear analyses and applies for both bifurcation and limit point instability, depending on what to appear on the equilibrium path. The proposed procedure for nonlinear buckling analysis is schematically shown in Fig. 1 and consists of the steps stated in Algorithm 1. During a geometrically nonlinear analysis the fundamental stability point is detected if it exists. Two stability situations are depicted in Fig. 1, an unstable bifurcation point and a load limit point. In both cases the stability point is detected by the procedures described in Section 2.2.

Algorithm 1 Pseudo code for the nonlinear buckling analysis

1: Geometrically nonlinear (GNL) analysis by arc-length method

2: Monitor and detect stability point during GNL analysis

3: Re-set all state variables to configuration at load step just before stability point - a precritical point

4: Perform eigenbuckling analysis on deformed configuration at load step before stability point
---

Let us consider geometrically nonlinear behaviour of structures made of linear elastic materials. We adopt the Total Lagrangian approach, i.e. displacements refer to the initial configuration, for the description of geometric nonlinearity.
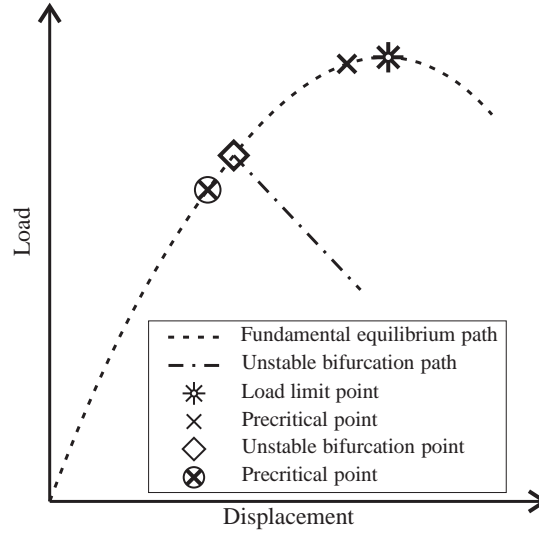
Figure 1: Detection of stability point in step 2 and chosen precritical equilibrium point for the nonlinear buckling problem in case of unstable bifurcation and limit point instability.

An incremental formulation is more suitable for nonlinear problems and it is assumed that the equilibrium at load step n is known and it is desired at load step $n + 1$. Furthermore, it is assumed that the current load is independent on deformation. The incremental equilibrium equation in the Total Lagrangian formulation is written as (see e.g. [40, 41])

$$\mathbf{K_T}(\mathbf{D}^n, \gamma^n)\,\delta\mathbf{D} = \mathbf{R}^{n+1} - \mathbf{F}^n \tag{1}$$

$$\text{where} \quad \mathbf{K_T}(\mathbf{D}^n, \gamma^n) = \mathbf{K_0} + \mathbf{K_L}(\mathbf{D}^n, \gamma^n) + \mathbf{K}_\sigma(\mathbf{D}^n, \gamma^n) \tag{2}$$

$$\text{i.e.} \quad \mathbf{K_T}^n = \mathbf{K_0} + \mathbf{K_L}^n + \mathbf{K}_\sigma^n \tag{3}$$

Here $\delta\mathbf{D}$ is the incremental global displacement vector, $\mathbf{F}^n$ global internal force vector, and $\mathbf{R}^{n+1}$ global applied load vector. The global tangent stiffness $\mathbf{K_T}^n$ consists of the global initial stiffness $\mathbf{K_0}$, the global stress stiffness $\mathbf{K}_\sigma^n$, and the global displacement stiffness $\mathbf{K_L}^n$. The applied load vector $\mathbf{R}^n$ is controlled by the stage control parameter (load factor) γ^n according to an applied reference load vector $\mathbf{R}$

$$\mathbf{R}^n = \gamma^n\mathbf{R} \tag{4}$$

The incremental equilibrium equation (1) is solved by the spherical arc-length method after [4, 42].

During the nonlinear path tracing analysis we can at some converged load step estimate an upcoming critical point, i.e. bifurcation or limit point, by utilizing tangent information. At a critical point the tangent operator is singular

$$\mathbf{K_T}(\mathbf{D}^c, \gamma^c)\boldsymbol{\phi}_j = \mathbf{0} \tag{5}$$

where the superscript c denotes the critical point and $\boldsymbol{\phi}_j$ the buckling mode. To avoid a direct singularity check of the tangent stiffness, it is easier to utilize tangent information at some converged load step n and extrapolate it to the

critical point. The one-point approach only utilizes information at the current step and extrapolates by only one point. The stress stiffness part of the tangent stiffness at the critical point is approximated by extrapolating the nonlinear stress stiffness from the current configuration as a linear function of the load factor γ.

$$\mathbf{K}_\sigma(\mathbf{D}^c, \gamma^c) \approx \lambda \mathbf{K}_\sigma(\mathbf{D}^n, \gamma^n) = \lambda \mathbf{K}_\sigma^n \tag{6}$$

It is assumed that the part of the tangent stiffness consisting of $\mathbf{K}_L^n$ and $\mathbf{K_0}$ does not change with additional loading, which holds if the additional displacements are small. The tangent stiffness at the critical point is approximated as

$$\mathbf{K_T}(\mathbf{D}^c, \gamma^c) \approx \mathbf{K_0} + \mathbf{K}_L^n + \lambda \mathbf{K}_\sigma^n \tag{7}$$

and by inserting into (5) we obtain a generalized eigenvalue problem

$$\left(\mathbf{K_0} + \mathbf{K}_L^n\right)\boldsymbol{\phi}_j = -\lambda_j \mathbf{K}_\sigma^n \boldsymbol{\phi}_j \tag{8}$$

where the eigenvalues are assumed ordered by magnitude such that λ_1 is the lowest eigenvalue and $\boldsymbol{\phi}_1$ the corresponding eigenvector. The solution to (8) yields the estimate for the critical load factor at load step n as

$$\gamma_j^c = \lambda_j \gamma^n \tag{9}$$

If $\lambda_1 < 1$ the first critical point has been passed and in contrary $\lambda_1 > 1$ the critical point is upcoming. The one-point procedure works well for both bifurcation and limit points. The closer the current load step gets to the critical point, the better the approximation becomes, and it converges to the exact result in the limit of the critical load.

In general, for engineering shell structures, the eigenvalue problem in (8) can be difficult to solve, due to the size of the matrices involved and large gaps between the distinct eigenvalues. For efficient and robust solutions, (8) is solved by a subspace method with automatic shifting strategy, Gram-Schmidt orthogonalization, and the sub-problem is solved by the Jacobi iterations method, see [43].

Traditional linear buckling analysis may be considered as a simplified version of the more general nonlinear buckling problem in (8). In linear buckling analysis the structure is assumed to be perfect with no geometric imperfections, stresses are proportional to the loads, displacements at the stability point are small, and the load to be independent of the displacements. Based on these assumptions on linearity the stress stiffening effects due to mechanical loading can be evaluated in terms of the displacements determined by a linear static analysis and a simplified version of the generalized eigenvalue problem in (8) can be established where the displacement stiffness of the system is neglected.

2.2. Detection of critical points

To obtain a good approximation of the critical load by nonlinear buckling analysis the precritical point used for the approximation have to be located in the neighbourhood of the critical load. In order to choose a good precritical point it is therefore necessary to detect stability points during the geometrically nonlinear analysis. Limit points are easily detected by monitoring the load factor in the GNL analysis, as stated in Algorithm 2. When the load factor from two

---

Algorithm 2 Pseudo code for limit point detection during GNL analysis

1: **if** $\gamma^n < \gamma^{n-1}$ **then**

2:     Define: $\gamma^{n-1} \equiv \gamma^c_{lim}$

3: **end if**

---

successive load steps decreases the previous converged load factor is defined as the limit load, i.e. $\gamma^{n-1} \equiv \gamma^c_{lim}$, and the precritical point for the nonlinear buckling analysis is then γ^{n-2}.

Bifurcation points are harder to detect than limit points. Here nonlinear buckling analysis according to (8) is performed at precritical stages during the geometrically nonlinear analysis as a singularity check on the tangent stiffness. When the critical load factor determined by the nonlinear buckling analysis is less than the current load factor, i.e. $\lambda_1 < 1.0$, a critical point has been passed. If the point is not defined as a limit point by the procedure in Algorithm 2 and the fundamental eigenvalue from solving the nonlinear buckling problem from two successive load steps is less than one, the stability point is defined as a bifurcation point. The procedure applied in this study for detecting bifurcation points is stated in Algorithm 3.

Algorithm 3 Pseudo code for bifurcation point detection during GNL analysis

1: **if** $n = 1$ **or** $\gamma^n \geq 0.9 \cdot {}^{nApp}\gamma^c_1$ **or** $n - nApp \geq nAppMax$ **then**

2:     Set: $nApp = n$

3:     Compute: $\left(\mathbf{K_0} + \mathbf{K^n_L}\right)\boldsymbol{\phi}_j = -\lambda^n_j\,\mathbf{K^n_\sigma}\,\boldsymbol{\phi}_j$

4:     Compute: ${}^{nApp}\gamma^c_1 = \lambda^n_1\,\gamma^n$

5:     **if** $\lambda^n_1 < 1.0$ **and** $\lambda^{n-1}_1 < 1.0$ **then**

6:         Define: $\gamma^{n-2} \equiv \gamma^c_{bif}$

7:     **end if**

8: **end if**

A nonlinear buckling analysis is always performed for the first converged equilibrium point. In order not to perform nonlinear buckling analysis for every converged equilibrium point during the GNL analysis some restrictions have been added, see Algorithm 3. A nonlinear buckling analysis is performed if the current load factor γ^n is larger or equal to 90% of the value of the critical load factor ${}^{nApp}\gamma^c_1$ determined at the previous approximation load step, $nApp$, according to the one-point approach. Furthermore, a nonlinear buckling analysis is performed if the number of load steps since the previous nonlinear buckling analysis exceeds $nAppMax$. If the fundamental eigenvalue from the nonlinear buckling problem from two successive load steps is less then one, the previous converged load factor associated with a fundamental eigenvalue larger than one is defined as the bifurcation load, i.e. $\gamma^{n-2} \equiv \gamma^c_{bif}$, and the precritical point for the nonlinear buckling analysis becomes γ^{n-3}.

With the implemented detection features there is a possibility of a special situation. If the arc-length solver during

7

geometrically nonlinear analysis automatically branches to an unstable bifurcated solution, the critical point will be detected as a limit point and not as a bifurcation point. This will however not influence upon the nonlinear buckling optimization procedure and thus the optimization result since the same equations for nonlinear buckling analysis and design sensitivity analysis apply for limit points and bifurcation points. During the numerical studies such a special situation did not occur.

2.3. Re-initialization of arc-length solver

For effective solution of the nonlinear buckling problem, i.e. geometrically nonlinear analysis, detection of stability points, and nonlinear eigenbuckling analysis, a re-initialization feature has been incorporated into the arc-length solver such that large load steps may be applied for the first part of the equilibrium path and reduced in the area of an upcoming stability point. Thus, a better resolution of the equilibrium path is obtained in the area of interest and a better precritical equilibrium point may be detected. The procedure is stated in Algorithm 4.

Algorithm 4 Pseudo code for re-initialization of arc-length

1: **if** $\gamma^n \geq 0.9 \cdot {}^{Oprev}\gamma_1^c$ **then**

2:     Reset arc-length with or without adaptivity

3: **end if**

${}^{Oprev}\gamma_1^c$ is the fundamental buckling load factor from the previous optimization iteration. The arc-length in the arc-length solver can either be set statically having the same value at all load steps or adaptively modified depending on the number of sub-iterations required for each load step. This adaptivity may be turned on or off during the re-initialization of the arc-length in the arc-length solver.

3. Design Sensitivity Analysis and Optimization of the Nonlinear Buckling Problem

To accomplish gradient-based optimization of the nonlinear buckling load factors, the nonlinear buckling load factor sensitivities must be derived. Only simple eigenvalues of conservative load systems are considered, but sensitivities of multiple eigenvalues can be computed using the approach described in, e.g., [44].

3.1. Design sensitivity analysis of simple eigenvalues

The eigenvalue problem in (8) is a generalized eigenvalue problem of the form

$$\mathbf{K}\boldsymbol{\phi}_j = \lambda_j \mathbf{M}\boldsymbol{\phi}_j, \quad j = 1, 2, \ldots, J \tag{10}$$

It is assumed that the eigenvectors are $\mathbf{M}$-orthonormalized, i.e. $\boldsymbol{\phi}_j^T \mathbf{M}\boldsymbol{\phi}_j = 1$. This means that $\boldsymbol{\phi}_j^T \left(-\mathbf{K}_\sigma^n\right)\boldsymbol{\phi}_j = 1$. In order to obtain the eigenvalue sensitivities, (8) is differentiated with respect to any design variable, $a_i, i = 1, \ldots, I$,

assuming that λ_j is simple.

$$\frac{d\lambda_j}{da_i}\left(-\mathbf{K}_\sigma^n\right)\boldsymbol{\phi}_j = \left(\frac{d\mathbf{K_0}}{da_i} + \frac{d\mathbf{K_L^n}}{da_i} - \lambda_j\frac{d\left(-\mathbf{K}_\sigma^n\right)}{da_i}\right)\boldsymbol{\phi}_j \tag{11}$$
$$+ \left(\mathbf{K_0} + \mathbf{K_L^n} - \lambda_j\left(-\mathbf{K}_\sigma^n\right)\right)\frac{d\boldsymbol{\phi}_j}{da_i}$$

By pre-multiplication of $\boldsymbol{\phi}_j^T$, make use of the $\mathbf{M}$-orthonormality of the eigenvectors, the governing equation (8), and noting that the system matrices are symmetric we obtain the eigenvalue sensitivities as

$$\frac{d\lambda_j}{da_i} = \boldsymbol{\phi}_j^T\left(\frac{d\mathbf{K_0}}{da_i} + \frac{d\mathbf{K_L^n}}{da_i} + \lambda_j\frac{d\mathbf{K_\sigma^n}}{da_i}\right)\boldsymbol{\phi}_j \tag{12}$$

In order to determine the eigenvalue sensitivity $\frac{d\lambda_j}{da_i}$ for any of the design variables a_i, $i = 1, \dots, I$, the derivative of the element initial stiffness matrix, element displacement stiffness matrix, and the element stress stiffness matrix have to be derived, respectively. These derivatives are calculated semi-analytically utilizing central difference approximations on element level and assembled to global matrix derivatives. This approach has been chosen as it is computationally efficient, easier to implement than analytical sensitivities and in case of fiber angle design variables there are no accuracy problems.

$$\frac{d\mathbf{k_0}}{da_i} \approx \frac{\mathbf{k_0}(a_i + \Delta a_i) - \mathbf{k_0}(a_i - \Delta a_i)}{2\Delta a_i} \tag{13}$$

$$\frac{d\mathbf{K_0}}{da_i} = \sum_{n=1}^{N_e^{as}} \frac{d\mathbf{k_0}}{da_i}, \quad i = 1, \dots, I \tag{14}$$

$\mathbf{k_0}$ is the element stiffness matrix, Δa_i is the design perturbation, and N_e^{as} is the number of elements in the finite element model associated to the design variable a_i.

Both the stress stiffness matrix and the displacement stiffness matrix are implicit functions of the displacements, i.e. $\mathbf{K}_\sigma^n = \mathbf{K}_\sigma\left(\mathbf{D}^n(\mathbf{a}), \mathbf{a}\right)$ and $\mathbf{K_L^n} = \mathbf{K_L}\left(\mathbf{D}^n(\mathbf{a}), \mathbf{a}\right)$, which must be considered. The design sensitivities of $\frac{d\mathbf{K_L^n}}{da_i}$ and $\frac{d\mathbf{K_\sigma^n}}{da_i}$ are evaluated semi-analytically by central finite difference approximations on the element level by

$$\frac{d\mathbf{k}_\sigma^n}{da_i} \approx \frac{\mathbf{k}_\sigma^n(a_i + \Delta a_i, \mathbf{D}^n + \Delta\mathbf{D}^n) - \mathbf{k}_\sigma^n(a_i - \Delta a_i, \mathbf{D}^n - \Delta\mathbf{D}^n)}{2\Delta a_i} \tag{15}$$

where the displacement increment is $\Delta\mathbf{D}^n \approx \frac{d\mathbf{D}^n}{da_i}\Delta a_i$. Thus, the displacement sensitivity, $\frac{d\mathbf{D}^n}{da_i}$, must be computed. At the converged load step n, we can write the equilibrium equation as

$$\mathbf{Q}^n(\mathbf{D}^n(\mathbf{a}), \mathbf{a}) = \mathbf{F}^n - \mathbf{R}^n = \mathbf{0} \tag{16}$$

where $\mathbf{Q}^n(\mathbf{D}^n(\mathbf{a}), \mathbf{a})$ is the so-called residual or force unbalance. Taking the total derivative of this equilibrium equation, with respect to any of the design variables a_i, $i = 1, \dots, I$, we obtain

$$\frac{d\mathbf{Q}^n}{da_i} = \frac{\partial\mathbf{Q}^n}{\partial a_i} + \frac{\partial\mathbf{Q}^n}{\partial\mathbf{D}^n}\frac{d\mathbf{D}^n}{da_i} = \mathbf{0} \tag{17}$$

$$\text{where} \quad \frac{\partial\mathbf{Q}^n}{\partial\mathbf{D}^n} = \frac{\partial\mathbf{F}^n}{\partial\mathbf{D}^n} - \frac{\partial\mathbf{R}^n}{\partial\mathbf{D}^n} \tag{18}$$

$$\text{and} \quad \frac{\partial\mathbf{Q}^n}{\partial a_i} = \frac{\partial\mathbf{F}^n}{\partial a_i} - \frac{\partial\mathbf{R}^n}{\partial a_i} \tag{19}$$

9

We note that (18) reduces to the tangent stiffness matrix. Since it was assumed that the current load is independent on deformation, $\frac{\partial \mathbf{R}^n}{\partial \mathbf{D}^n} = \mathbf{0}$, we obtain

$$\frac{\partial \mathbf{F}^n}{\partial \mathbf{D}^n} = \mathbf{K}_\mathbf{T}^n \tag{20}$$

By inserting the tangent stiffness and (19) into (17), we obtain the displacement sensitivities $\frac{d\mathbf{D}^n}{da_i}$ as

$$\mathbf{K}_\mathbf{T}^n \frac{d\mathbf{D}^n}{da_i} = \frac{\partial \mathbf{R}^n}{\partial a_i} - \frac{\partial \mathbf{F}^n}{\partial a_i} \tag{21}$$

For design independent loads, the term $\frac{\partial \mathbf{R}^n}{\partial a_i} = \mathbf{0}$.

Thus, all terms have been derived for the evaluation of the eigenvalue sensitivities in (12) and the estimate for the nonlinear buckling load factor sensitivity at load step n is

$$\frac{d\gamma_j^c}{da_i} = \frac{d\lambda_j}{da_i}\gamma^n \tag{22}$$

3.2. The mathematical programming problem

The mathematical programming problem for maximizing the lowest critical load is a max-min problem. The direct formulation formulation of the optimization problem can give problems related to differentiability and fluctuations during the optimization process since the eigenvalues can change position, i.e. the second lowest eigenvalue can become the lowest. An elegant solution to this problem is to make use of the so-called bound formulation, see [45], [46], and [47]. A new artificial variable β is introduced and a new artificial objective function β is chosen. An equivalent problem is formulated, where the previous non-differentiable objective function is transformed into a set of constraints. The optimization formulation in the case of laminate optimization, for a max-min problem with the use of the bound approach, is formulated as follows

$$\text{Objective :} \quad \max_{\boldsymbol{x}, \beta} \beta$$

$$\text{Subject to :} \quad \gamma_j^c \geq \beta, \quad j = 1, \ldots, N_\lambda$$

$$\left(\mathbf{K_0} + \mathbf{K_L}^n + \lambda_j^n \mathbf{K_\sigma}^n\right)\boldsymbol{\phi}_j^n = \mathbf{0}$$

$$\gamma_j^c = \lambda_j^n \gamma^n$$

$$\underline{x_i} \leq x_i \leq \overline{x_i}, \quad i = 1, \ldots, I$$

where x_i denote the laminate design variables in terms of fiber angles.

The mathematical programming problem is solved by the Method of Moving Asymptotes (MMA) by [48]. The closed loop of analysis, design sensitivity analysis and optimization is repeated until convergence in the design variables or until the maximum number of allowable iterations has been reached.

## 4. The Cylindrical Shell Benchmark Problem and Solutions

The cylindrical shell panel example was first introduced by [5] and later appeared in numerous journal articles. The example has been used as a benchmark to investigate advances in numerical finite elements methods for handling load and/or deflection reversals in nonlinear buckling problems. Furthermore, it is used to demonstrate the capability of finite element procedures to traverse such complicated load paths.

Lately, [6, 7] noticed that the solution by [5] and re-produced by many other authors through several decades is incorrect. The incorrect solution only involves symmetric deformation modes and makes the assumption that limit point buckling occurs. [6, 7] discovered through numerical studies and related experiments that the former symmetric solution is incorrect and the existence of bifurcation and asymmetric buckling mode at a lower load level. Furthermore, [6, 7] concludes that the bifurcation point is stable which means that the structure is able to carry more load after bifurcation until, according to [6, 7], a load limit point instability is encountered. The results by [6, 7] is also included and discussed in the book by [8]. Their conclusion about the stability of the bifurcation point turns out to be incorrect, i.e. the bifurcation point is not stable but unstable.

Both the incorrect symmetric and the correct asymmetric solution to the benchmark example are presented in order to clarify the complicated behaviour that may be encountered in shell buckling for even an immediate simple well-known example. The complicated buckling behaviour for the numerical example will therefore pinpoint some of the challenges in optimizing geometrically nonlinear structures with respect to a general type of stability. Furthermore, the stability of the bifurcation point from the asymmetric solution is analysed and the results from [6, 7] is disproved by numerical results from simulations based on an in-house FE and optimization code called the MUltidisciplinary Synthesis Tool (MUST [49]) and the commercial FE program ANSYS [50].

The benchmark problem is an isotropic thin circular cylindrical shell panel of square planform, transversely point loaded, undergoing large deformations including buckling and post-buckling. Material and geometric properties for the benchmark problem are given in Fig. 2.

The panel is supported by its two straight axial edges having a pinned fixture that cannot move, i.e. hinged. The panel is free on the curved circumferential edges. The hinged constraint is represented in the model by multi point constraints between the top and bottom edge nodes, i.e. the mid-surface of the axial edges is restrained in displacements and rotations in u, v, w, R_x, R_y but free to rotate about the z-axis (R_z). In the analysis, the shell is transversely point-loaded at the center of the shell panel, which is applied by two point loads in the negative y-direction, at the top and bottom node in the centre of the panel. Symmetry considerations have deliberately not been enforced since a full model is required to fully investigate bifurcation buckling. The model consists of 400 equivalent single layer solid shell finite elements which through mesh convergence studies have been determined sufficient for adequately capturing the load-deflection and mode evolutions for the benchmark problem.

11
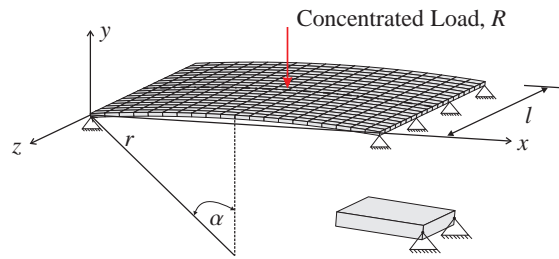
$r = 2540mm$	$E = 3.10275GPa$	$G = 1.19337GPa$
$l = 508mm$	$t = 6.35mm$	$v = 0.3$
$\alpha = 0.1rad$	$S = 508mm$	$R = 2400N$

Figure 2: Geometry, loads, boundary conditions, and material properties for the cylindrical shell example. The hinged support is related to the mid surface of the shell, which is realized by multi point constraints between the top and bottom edge nodes of the solid shell finite elements. The shell is loaded by two point loads in the negative *y*-direction, at the top and bottom node in the centre of the shell. The top node in the centre of the panel is constrained against displacements in the *x*- and *z*-direction. All dimensions refer to the mid surface, where the thickness is denoted by *t*. The shell centerline is also marked on the figure and is represented by the bottom mesh grid points.

4.1. Symmetric Solution

The load versus center deflection response from a geometrically nonlinear analysis upon the original perfect system is presented in Fig. 3 together with the original solution by [5] and the symmetric solution in [6, 7]. The solutions are in almost perfect agreement.
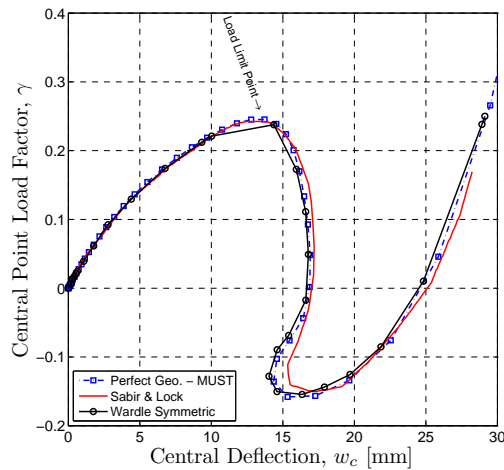

Figure 3: Load-deflection response solutions of the perfect symmetric system.

Both load and deflection are taken positive in the loading direction. The stability limit is characterized by a load limit point at a load limit of $R_{LP} \approx 588N$. A path tracing algorithm is needed for this solution as both load- and deflection reversals occur. Snap-through would occur at the load limit point in load control, and snap-down at the deflection limit point in deflection control. The path tracing algorithm called the arc-length method after [4] is applied

12

in this work.

Spanwise mode shapes along the shell centerline obtained by MUST are presented in Fig. 4 for several values of center deflection, w_c. Line markers on this deformation plot are the bottom mesh grid points of the shell.
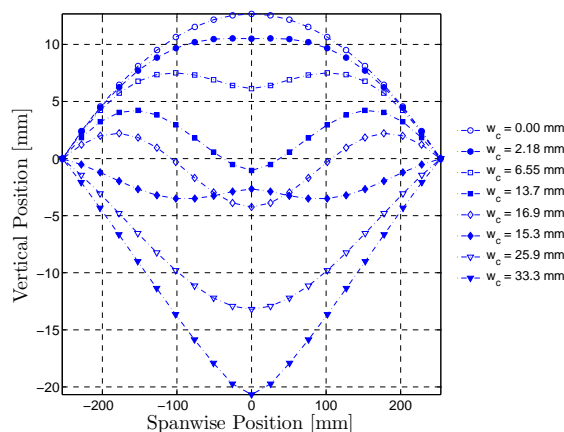

Figure 4: Central spanwise mode shapes at different values of center deflection, w_c, obtained by FEA on the perfect symmetric system.

The spanwise mode shapes are symmetric about the centerline and loading point. After reaching the deflection limit point at $w_c \approx 16.9mm$ a snap-back occurs where both load and center deflection decrease simultaneously. At larger values of center deflection, the shell is fully inverted (concave, rather than the convex undeformed shape) and begins to act like a stretched membrane. This is also evident on the load-deflection behaviour in Fig. 3 where slight nonlinear stiffening is observed for center deflections larger than $w_c \approx 22mm$.

4.2. Asymmetric Solution

The symmetric solution of the problem makes the assumption that limit point buckling will occur and does not consider bifurcation and associated asymmetric buckling mode. Most analyses make this implicit assumption by symmetry considerations with respect to geometry, loading and response by which only 1/4 of the shell is modelled. [6, 7] noticed that the symmetric solution was incorrect and that there exists a asymmetric solution in terms of bifurcation at a lower load than the load limit point for the symmetric solution.

Four different techniques are applied in this study in order to determine the bifurcation point and the associated bifurcated path. The precisions of the different techniques are compared individually and to the asymmetric solution by [6, 7]. The four techniques applied to obtain the asymmetric solution are classified as

1. Linear buckling analysis

2. GNL analysis of imperfect system

3. Nonlinear buckling analysis at deformed configurations on perfect system

4. GNL analysis by arc-length method of perfect system with small step size

13

In engineering applications linear buckling analysis is often used as a generalized stability predictor for shell structures, see e.g. [51]. Within linear buckling analysis the structure is assumed to behave linearly up until the buckling point neglecting all types of nonlinearity. For some cases, despite whether the critical point is a bifurcation or limit point, the classical theory yields a satisfactory prediction of the buckling load while it in other cases gives results of little or no value. Typically, linear buckling analysis gives poor predictions of limit point instability since that type of instability inherently is nonlinear. Since the structures analyzed with linear buckling analysis are perfect with no imperfections of any kind together with the assumptions involved in the theory, the prediction will typically be an upper limit for the real collapse load, and the method is therefore in literature often stated as non-conservative in an engineering context, see e.g. [52].

The buckling load estimated by linear buckling analysis is $R_{LB} = 674N$ and the associated buckling mode is shown in Fig. 5.
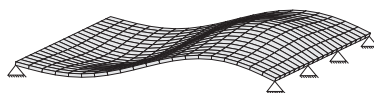

Figure 5: 1$^{\text{st}}$ buckling mode shape obtained by linear buckling analysis.

The buckling mode from linear buckling analysis is asymmetric and corresponds to bifurcation buckling. Comparing this buckling load, $R_{LB} = 674N$, with the limit point buckling load of the symmetric system, $R_{LP} \approx 588N$, it seems that bifurcation buckling will not occur prior to the load limit point. In order to precisely verify that bifurcation does not occur the second technique is applied. A slightly distorted/imperfect system is analysed in order to investigate whether a secondary equilibrium path exist. This may be accomplished by introducing geometric imperfections in the shell geometry in the form of the first linear buckling mode with a specified amplitude. The amplitude is defined as the largest translational component of the first linear buckling mode relative to the thickness of the shell. Geometrically nonlinear analysis of the imperfect system may reveal whether bifurcation occurs onto a secondary bifurcated equilibrium path. Equilibrium paths of imperfect systems with different relative imperfection size in relation to the thickness of the shell are shown in Fig. 6. All equilibrium paths from the imperfect systems follow a different path than the one from the perfect system, thus a bifurcation branch exist.

From the solutions of the imperfect systems the problem of choosing appropriate imperfections and size for analyzing bifurcation points is apparent. The imperfection size has to be lower than approximately 1% in order not to change the problem and thereby the solution. Thus the imperfection amplitude has to be large enough to induce bifurcation but also small enough not to change the problem. At approximately 516N, the shell bifurcates onto a secondary branch associated with a dominant asymmetric mode, see Fig. 7.

Bifurcation occurs about 12% below the load limit point for the symmetric solution, thus this is the preferred lower energy path. The two reliable imperfect equilibrium paths (0.1% & 1% Imperfect Geo.) show a limit point in the region of the bifurcation point and do not exhibit a deflection limit point but rejoins the equilibrium path with the symmetric response at large values of center deflection. In this region the response is dominated by membrane
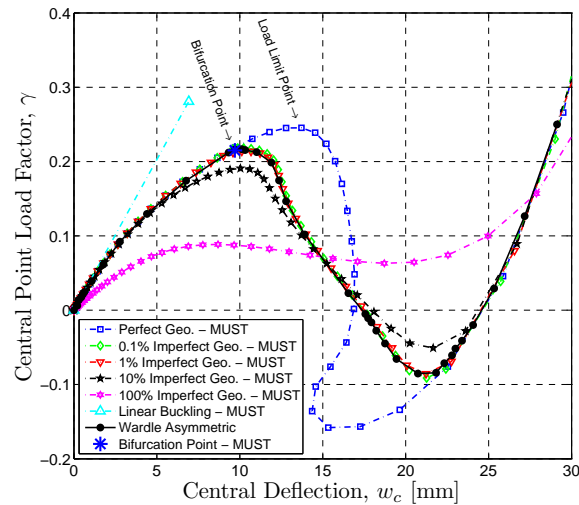
14

Figure 6: Load-deflection response solutions of the perfect and imperfect system together with the linear buckling load.

stretching with symmetric modes, see Fig. 7. [6, 7] obtained an almost identical solution by inducing imperfections by the so-called asymmetric meshing technique (AMT) and subsequent geometrically nonlinear analysis, see Fig. 6.

In order to determine the bifurcation load more precisely the third technique is applied. The equilibrium path is traced by Newton's method with a fixed load step size of 1%. At each converged iteration a nonlinear buckling analysis, see Section 2, is performed on the current deformed configuration as a singularity check on the tangent stiffness. From this technique the bifurcation point is determined to be between 504 and 528N. The bifurcation point is marked on Fig. 6 as 516N.

Applying the fourth technique the bifurcated path is determined by geometrically nonlinear analysis of the perfect system, i.e. without introducing any imperfections. The equilibrium path is traced by the arc-length method and at a load step close the bifurcation point the arc-length, controlling the step size in the arc-length method, is reduced dramatically and the step size adaptivity is removed. With such a small step size it is possible to trace the branching from the fundamental to the secondary bifurcated path as shown in Fig. 8.

By the solution in MUST the entire equilibrium paths are obtained by a single arc-length solution with very small arc-length step size. Initially, the fundamental path is traced up until the bifurcation point whereby the secondary path is traced. At the second bifurcation point the analysis returns to the fundamental path which is traced towards the lower load limit point and through the upper load limit point. At the first bifurcation point the analysis again returns to the secondary path. Reaching the second bifurcation point the analysis traces the remaining part of the fundamental equilibrium path.

The bifurcation point is accurately determined at a load level of 526N and it is quite clear that the bifurcation point is unstable, i.e. in load control the structure will at the bifurcation point experience a dynamic snap-through onto a stable configuration which is located on the fundamental equilibrium path, see Fig. 9. Due to the many iterations
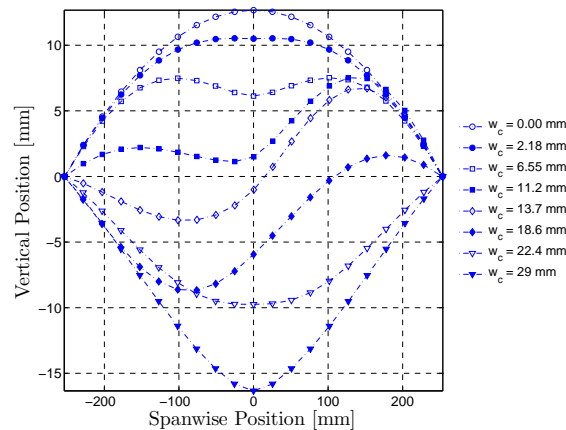
Figure 7: Central spanwise mode shapes at different values of center deflection, w_c, obtained by FEA on the imperfect system with imperfection amplitude of 0.1%.

needed by this procedure, more than 25.000 iterations for this example, this numerical procedure is not suited for real life problems. Furthermore, the location of the bifurcation point should be known a priori in order to activate the small step size and be chosen sufficiently small in order to branch to the secondary path. Otherwise a small arc-length step size has to be used also for the initial part of the fundamental equilibrium path which results in additional numerical cost.

This result has been verified by a similar model in ANSYS where 9-noded shell elements (Shell91) have been applied to model the cylindrical shell example. The bifurcated path is by ANSYS also obtained by geometrically nonlinear analysis by the arc-length method with a very small arc-length step size. The results from the shell model in ANSYS and the results from the solid shell model in MUST are in good agreement, see Fig. 8 and 9.

These results disprove the results published in [6, 7] and in [8] in which it is concluded that the bifurcation point is stable. [6, 7] and [8] conclude that the bifurcation point is stable, i.e. bifurcated path is stable and that the structure is able to accept more load until a load limit point on the bifurcated path is reached. This is not correct but probably just a wrong interpretation of the numerical results. The asymmetric solution in [6, 7] is obtained by geometrically nonlinear analysis of an imperfect system. It is correct that the stability limit of the equilibrium path for the imperfect system is characterized by a limit point but the bifurcation point for the imperfect system is non-existing. The bifurcation point of the perfect system is merely transformed into a limit point for the imperfect structure. This statement may also be verified by comparing the limit point load 523.4*N* for the imperfect system with the accurately determined bifurcation load 526*N* of the perfect system. Thus the bifurcation point is unstable and not stable as stated in [6, 7, 8].

In Fig. 10, a three dimensional plot of the equilibrium paths are given. The central point load factor is plotted against the vertical central point deflection, w_c, and the central point rotation about the z-axis, $R_{z,c}$, respectively. The central point rotation is calculated by the deflections of a couple of neighbouring nodes. The rotation is a measure for non-symmetric bifurcation mode shape evolutions during loading.
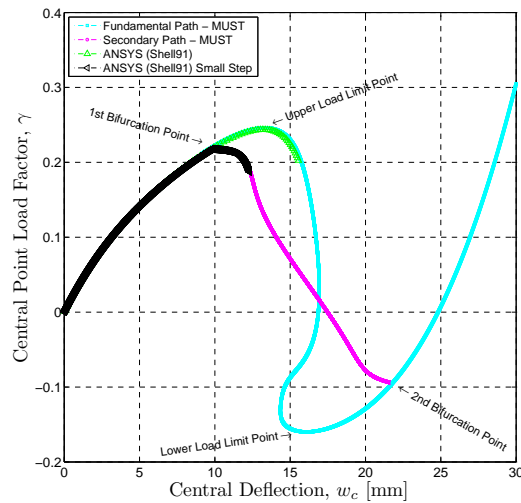
16

Figure 8: Load-deflection curves of the perfect symmetric system for both the fundamental equilibrium path and the secondary bifurcated path obtained by MUST and a shell finite element model in ANSYS.

In the load-deflection plane there is the already discussed limiting behaviour on the fundamental equilibrium path given by the load limit point, but before the corresponding instability with respect to w_c is encountered a bifurcation of equilibrium into the asymmetric bifurcation mode at the point marked on the figure takes place.

Initially the shell deflects symmetrically with w_c increasing nonlinearly with loading, γ, and rotation $R_{z,c}$ equal to zero. An unstable symmetric point of bifurcation is reached at the marked point and the shell will snap dynamically through non-symmetric states typified by $R_{z,c} \neq 0$ to a stable configuration on the fundamental equilibrium path. From projections of the equilibrium paths in the load-rotation plane it may be observed that non-symmetric mode shape evolutions grow and decrease quickly near the first and second point of bifurcation. In the load-deflection plane the two bifurcated paths coincide and correspond to Fig. 8 and the bifurcated paths do not exhibit a deflection limit point, i.e. the bifurcated paths are stable in defection control.

5. Nonlinear Buckling Optimization of Composite Cylindrical Shell

A composite cylindrical shell example studied both numerically and experimentally by [53, 54] is considered for fiber angle optimization w.r.t. a general type of stability. Material and geometric properties for the benchmark problem are given in Fig. 11. The initial shell laminate consists of a graphite-epoxy (AS/3501-6) $[\pm 45°/0°]_s$ layup with an equal ply thickness of 0.134mm. Loading and boundary conditions are identical to the shell problem discussed previously. Symmetry considerations have deliberately not been enforced since a full model is required to fully investigate bifurcation buckling. The model again consists of 400 equivalent single layer solid shell finite elements which through mesh convergence studies have been determined sufficient for adequately capturing the buckling behaviour of the problem.
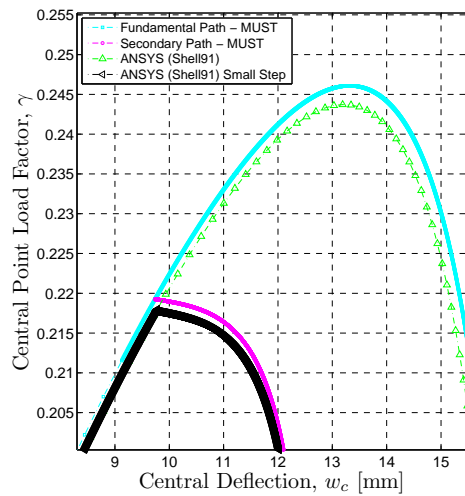
17

Figure 9: Zoomed view of the bifurcation and limit point. It is clear that the bifurcation point in unstable, i.e. the tangent is negative directly after bifurcation.
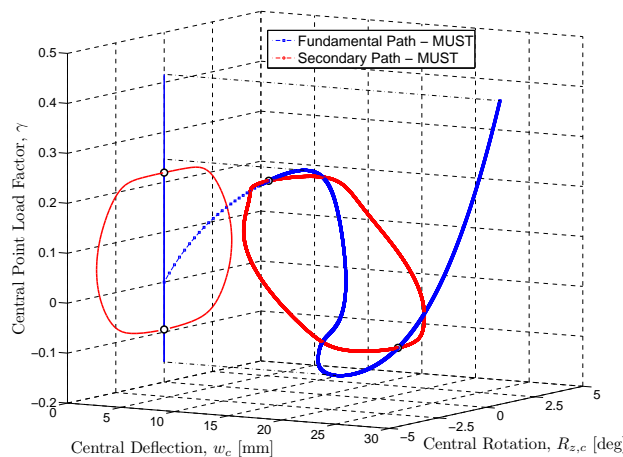

Figure 10: Equilibrium paths of the cylindrical shell in a three dimensional representation.

Various solutions to the initial design of the composite shell example are given in Fig. 12. The nonlinear equilibrium problem features both a limit point and a bifurcation point on the fundamental equilibrium path. The bifurcation point is reached prior to the limit point, thus this is the preferred lower energy path. The fundamental path may be obtained by path following techniques upon the perfect system, whereas the bifurcated path may be obtained by path following techniques upon an imperfect structure. Imperfections are applied as described in Section 4. For the imperfect system, the bifurcation point is transformed into a limit point since bifurcation is unstable. The bifurcation point may also be determined directly for the perfect system by using other techniques, e.g. by those described in Section 4. The geometrically nonlinear solution of the perfect system is denoted the symmetric solution, whereas the solution which involves the bifurcated equilibrium path is denoted the asymmetric solution.

The equilibrium paths obtained by the in-house analysis and optimization code MUST are in perfect agreement

$$
\begin{array}{lll}
r = 914.4mm & \alpha = 0.167rad & \nu_{12} = \nu_{23} = 0.3 \\
l = 304.8mm & E_1 = 142GPa & \nu_{13} = 0 \\
t = 0.804mm & E_2 = E_3 = 9.81GPa & R = 800N \\
S = 304.8mm & G_{12} = G_{13} = 6.00GPa &
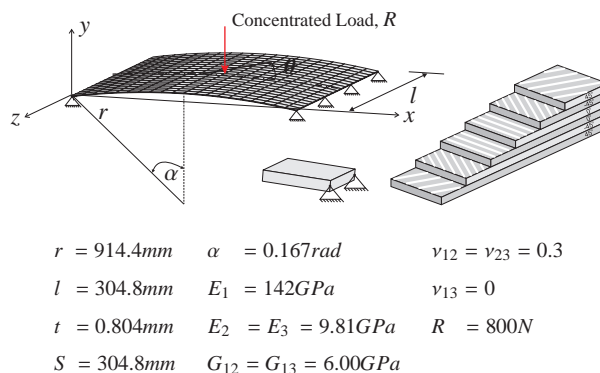\end{array}
$$

Figure 11: Geometry, loads, boundary conditions, material properties, laminate layup for the composite cylindrical shell example. The hinged support is related to the mid surface of the shell, which is realized by multi point constraints between the top and bottom edge nodes of the solid shell finite elements. The shell is loaded by two point loads in the negative y-direction, at the top and bottom node in the centre of the shell. The top node in the centre of the panel is constrained against displacements in the x- and z-direction. All dimensions refer to the mid surface, where the total thickness is denoted by t. The fiber angles for the laminate layup are measured by the angle, θ, from the shell centerline.

with a similar shell finite element model in ANSYS and numerical solutions from [54, 6, 7]. Linear buckling analysis yields a good prediction of the bifurcation load factor but a poor prediction of the displacements at bifurcation.

During optimization of the cylindrical composite shell several interesting things might take place. Considering the equilibrium paths in Fig. 12, optimization of the lowest stability load may push the bifurcation load towards the limit point and maybe even above it and as a consequence cause the bifurcation point to vanish. Furthermore, iterative design changes during optimization may also introduce some kind of non-symmetry into the structure in the same manner as geometric imperfections which changes the bifurcation point on the fundamental path to a limit point on the equilibrium path of the "imperfect" system. All these issues are taken care of in the general type nonlinear buckling optimization formulation presented in Section 2 and 3 and demonstrated by the following optimization cases.

5.1. Case #1 - Laminate Fiber Angle Optimization

The composite laminate shell is optimized with respect to a general type stability load, i.e. depending on the first stability point to appear on the fundamental equilibrium path, bifurcation point or limit point, that point is considered for optimization. The bound formulation is applied considering the lowest four buckling load factors in order to avoid problems related to mode switching, i.e. if e.g. the bifurcation point in Fig. 12 is pushed towards the load limit point. Fiber angles in the laminate layup definition are chosen as design variables and may vary continuously. This gives a total of 6 fiber angle design variables.

The starting point for the optimization is the initial laminate layup analyzed previously. The optimization history is shown in Fig. 13, where both the objective function value, i.e. the estimated critical point value in the nonlinear buckling analysis, and the detected critical point, i.e. bifurcation or limit point, are plotted for each optimization iteration.
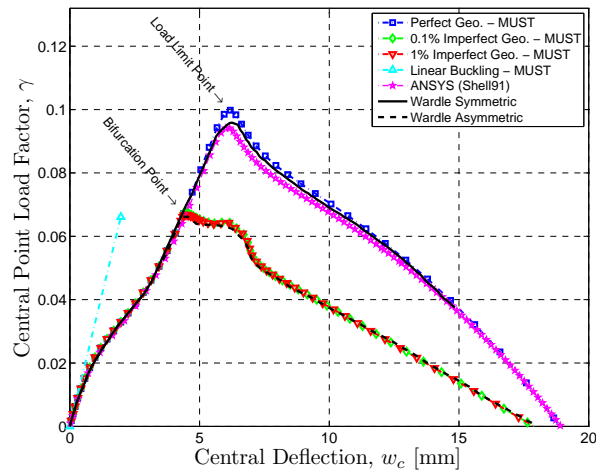
19

Figure 12: Load-deflection response solutions of the perfect symmetric system, solutions of different imperfect systems with varying imperfection amplitude, ANSYS Shell91 solution, numerical result from [54, 6, 7], and linear buckling solution.

During optimization the type of the stability point changes between being a bifurcation and a limit point and the optimization formulation successfully succeed to improve the general type stability load. The change in stability is caused by non-symmetry in the laminate design introduced by the optimizer. Introduction of non-symmetry in the laminate layup has the same effect as imperfections which were discussed in Section 4, i.e. it transforms the unstable bifurcation point into a limit point. The lowest buckling load factors do not get close during optimization thus no mode switching occur. The stability load of the optimized design is $188.1N$ and the optimized fiber angle design is $[0.6°/1.4°/-42.6°/43.4°/-2.2°/-1.1°]$.

Traditional linear buckling optimization, considering the lowest four linear buckling load factors, yields a different result, see the optimization histories in Fig. 14. The fundamental linear buckling load of the optimized design is $112.6N$ whereas the more accurately determined stability load predicted by geometrically nonlinear analysis yields a stability load of $158.5N$ of the linear buckling optimized design, thus linear buckling analysis severely underestimates the buckling load of the optimized design. The linear buckling optimized fiber angle design is $[3.7°/-25.0°/54.5°/-16.3°/-33.9°/13.2°]$.

During linear buckling optimization the lowest two buckling load factors gets close and mode switching occur, see Fig. 14. In order to take care about possible multiple eigenvalues the formulation described in [44] has been applied since multiple eigenvalues not are differentiable in the common sense and the sensitivities cannot be calculated in the same manner as for simple distinct eigenvalues. This formulation has only been applied when the difference between the eigenvalues is below 0.1%. Despite very close values between the two fundamental eigenvalues no multiplicity could be confirmed by inspection of the so-called generalized gradient vectors, see [44].

The two fundamental buckling modes for optimization iteration one predicted by linear buckling analysis are depicted in Fig. 14 and consist of an asymmetric and symmetric buckling mode. The asymmetric mode corresponds to bifurcation buckling whereas the symmetric mode corresponds to limit point buckling. It is interesting to note that the
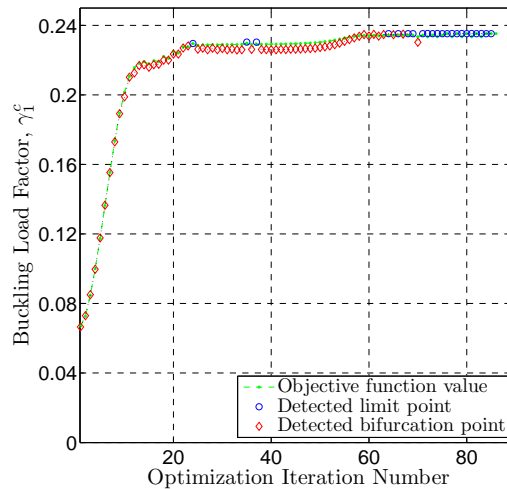
Figure 13: Optimization history of lowest buckling load factor in optimization case #1. The objective function value determined by nonlinear buckling analysis are plotted together with bifurcation and limit points detected during GNL analysis.

fundamental buckling mode during optimization switches between these modes, i.e. linear buckling analysis predicts for some design configurations limit point buckling. Important to notice is also that these buckling mode predictions are artefacts of the ability of the linear buckling formulation to predict stability, i.e. no multiple eigenvalues or close eigenvalues can be predicted by accurate geometrically nonlinear buckling analysis. Thus, geometrically nonlinear prebuckling effects play an important role for this example and unreliable buckling predictions are obtained by the linear buckling formulation. Furthermore, the general type nonlinear buckling optimization formulation yields a much better design for maximum buckling resistance.

For the nonlinear buckling optimization the re-initialization feature of the arc-length solver is activated during geometrically nonlinear analysis according to Algorithm 4, giving a total of $15 - 19$ load steps for each analysis. The re-initialization feature is activated at a load level of approximately 90% of the critical load resulting in typically $5 - 10$ load steps for the remaining part of the equilibrium path until the critical point is reached. The load level for the chosen equilibrium point for the nonlinear buckling analysis and design sensitivity analysis, see (8) and (12), is typically $2 - 4\%$ less than the critical load. To investigate the sensitivity of the nonlinear buckling optimization procedure with respect to the estimation point, the optimization is performed without the use of the re-initialization feature of the arc-length solver, resulting in a coarser solution resolution, i.e. less equilibrium points near the critical point. This results in $8 - 11$ load steps for the geometrically nonlinear analysis and an estimation point at a load around 25% less than the critical load. The stability load of the nonlinear buckling optimized design without re-initialization of the arc-length solver is $183.2N$, which only is slightly lower than the buckling load of the optimized design with the use of the re-initialization feature. Thus, for this example the nonlinear buckling optimization procedure is not very sensitive to the chosen precritical equilibrium point for nonlinear buckling analysis and design sensitivity analysis. However, a fine solution discretization is needed to accurately detect the critical point load.
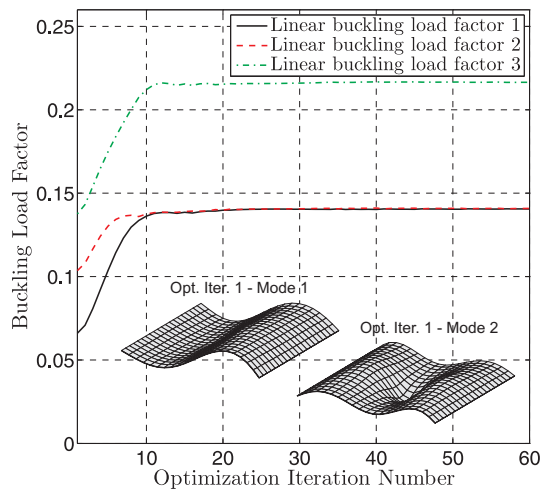
Figure 14: Linear buckling optimization histories of the three lowest buckling load factors and the two lowest stability modes at optimization iteration one.

5.2. Case #2 - Laminate Fiber Angle Optimization

For this optimization case the design parametrization are different from the previous optimization case #1 whereas the same optimization formulations are applied and studied. The shell is divided into 4 patches, see Fig. 15. Within a patch containing a set of finite elements only one fiber angle design variable controls the orientation of the given fiber layer in the finite element set. This is a valid approach for practical design problems since laminates are typically made using fiber mats covering larger areas. Having 4 patches and 6 fiber layers in the laminate layup thus gives a total of 24 fiber angle design variables. Though, this parametrization may yield discontinuities between fiber angles within the same laminate layer which may not be preferable from a manufacturing point of view. This problem could be circumvented with the application of manufacturing constraints.
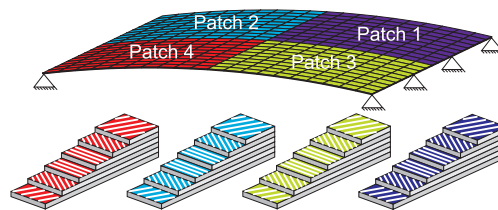

Figure 15: Parametrization for laminate fiber angle optimization of cylindrical composite shell in optimization case #2.

The starting point for the optimization is the initial laminate layup analyzed previously. The optimization history is shown in Fig. 16, where both the objective function value, i.e. the estimated critical point value in the nonlinear buckling analysis, and the detected critical point, i.e. bifurcation or limit point, are plotted for each optimization iteration.

During optimization the type of the stability point again changes between being a bifurcation and a limit point and the change in stability is again caused by non-symmetry in the laminate design introduced by the optimizer.
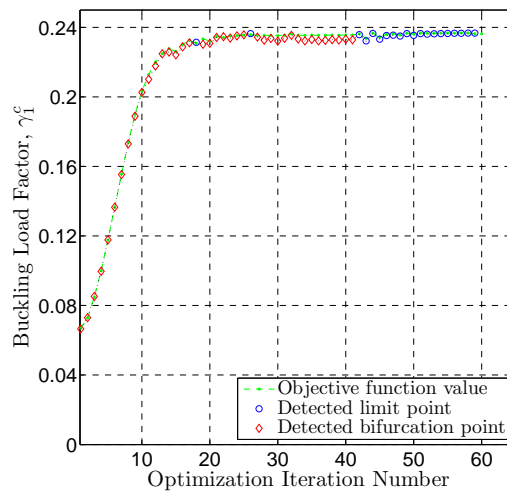
22

Figure 16: Optimization history of lowest buckling load factor in optimization case #2. The objective function value determined by nonlinear buckling analysis are plotted together with bifurcation and limit points detected during GNL analysis.

The stability load of the general type nonlinear buckling optimized design is 189.4N and thereby slightly higher than the stability load obtained in optimization case #1. This is meaningful since more design freedom exists for the parametrization applied in this optimization case and a better optimization result is expected. The linear buckling optimized design has a linear buckling load of 115.3N and a geometrically nonlinear stability load of 165.0N. Again, geometrically nonlinear prebuckling effects play an important role thus the linear buckling optimization formulation yields less performing optimization results and underestimates the stability load of the optimized design.

5.3. Case #3 - Single Layer Fiber Angle Optimization

The shell is now considered only having a single fiber layer of the total thickness. The fiber angle in each finite element is initially set to 90°. In the optimization the fiber angle is changed in each finite element giving a total of 400 fiber angle design variables. This parametrization is not entirely physical from a manufacturing point of view but gives large design freedom in the optimization, nice representation of the design results, and serves only as a numerical academic benchmark. Optimization is again performed with respect to the linear buckling load and the general type nonlinear buckling load and the results are compared in order to determine the importance of including nonlinear prebuckling effects in the optimization formulation. In each case the bound formulation is applied considering the lowest four buckling load factors.

The linear buckling optimized design has a linear buckling load of 133.7N and a geometrically nonlinear stability load of 163.1N, and the linear buckling optimized fiber angle design is shown in Fig. 19 left.

The optimization history to the general type nonlinear buckling optimization is shown in Fig. 17. As for the previous cases the stability type is dependent on symmetry in design, i.e. limit points are detected when the fiber angle layout is not perfectly symmetric where non-symmetry in the design is introduced by the optimizer. The optimized

23

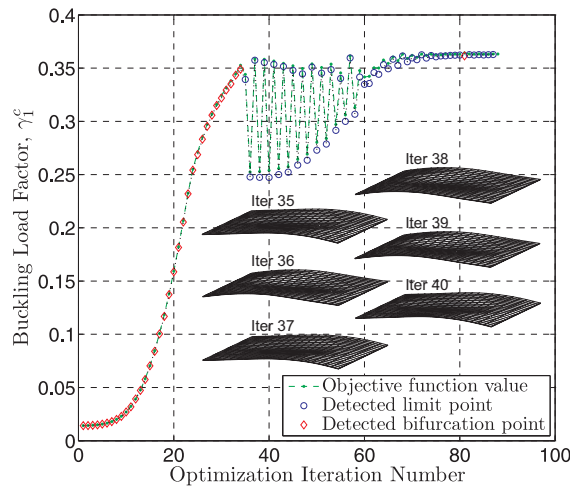design has a stability load of 290.2N and the optimized fiber angle design is shown in Fig. 19 right.

Figure 17: Optimization history of lowest buckling load factor in optimization case #2. The objective function value determined by nonlinear buckling analysis are plotted together with bifurcation and limit points detected during GNL analysis. Stability modes for optimization iterations $35 - 40$ are shwon.

During the optimization iterations $35 - 69$ major fluctuations occur in the detected stability load. The stability modes for the optimization iterations $35 - 40$ are shown in Fig. 17. It may be observed that the stability mode between iteration 35 and 36, 36 and 37, and 37 and 38, respectively, are totally opposite due to the bifurcated path taken for the unstable symmetric point of bifurcation, see e.g. Fig. 10 for reference. However, the stability mode between optimization iteration 38 and 39 are similar whereby the fluctuations in the optimization history cannot be explained solely by change in stability mode. In order to investigate this further, geometrically nonlinear analyses have been performed for the designs according to the optimization iterations $35 - 40$ and their equilibrium paths, in terms of load factor, γ, versus central point rotation, $R_{z,c}$, are plotted in Fig. 18.
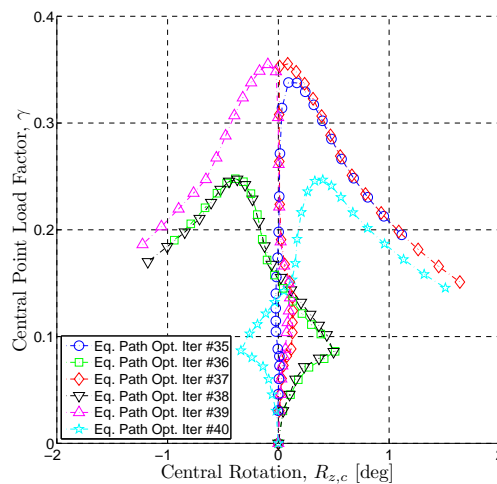

Figure 18: Equilibrium paths of the designs from optimization iteration $35 - 40$ in terms of load versus central point rotation.

24

It is immediately noticed that some of the designs have central point prebuckling rotations that are of opposite sign than the rotations at the stability point. The design from optimization iteration 37 has central point prebuckling rotations of same sign as the rotations of the stability point. The optimization iterations 36, 38, 40 have the largest central point prebuckling rotations of opposite sign and also the lowest stability loads. Yet, none of the above observations may explain the fluctuations in the optimization history. The relative design changes from the MMA optimizer in optimization iterations 35 − 69 differs from 0.06% − 0.99% having the largest design changes in the preliminary iterations and reduced to 0.06% in iteration 69. The largest design changes involve a maximum change in all fiber angles of approximately 3.6°. The reduction in design change is caused by adaptivity control of the maximum move limit of the design variables, i.e. the maximum move limit of a design variable is reduced if the design change from two successive optimization iterations is of opposite sign. However, relatively small design changes in the considered optimization iterations lead to major changes in the stability load. This indicates that the design space is highly non-linear in this design area. Fiber angle optimization is known to be associated with a non-convex design space with many local minima. Thus, the fluctuations may be avoided by reducing the maximum move limit, though increasing the risk of convergence to a local minimum. This has been attempted for the present optimization case and more smooth optimization histories were achieved on the expense of lower stability loads.

The general type nonlinear buckling optimized design is approximately 42.9% better than the linear buckling optimized design, thus geometrically nonlinear prebuckling effects play an important role for this example. This is also noticed by considering the optimized designs in Fig. 19. The pattern like designs of fiber angle distribution are very different despite that most of the fibers for both optimized designs are aligned in the circumferential direction.

Figure 19: Left: Linear buckling optimized design. Right: General type nonlinear buckling optimized design. The hinged supports are at the left and right edges of the panels.

The linear buckling optimization formulation succeeds improving the buckling load despite the inherent linear assumptions in the formulation and the poor prediction of the "real" stability load which at the optimized design were underestimated. Yet the general type nonlinear buckling optimization formulation proves to give much better optimization results, a more reliable prediction of the stability load, and information about the type of instability. Linear buckling optimization should be used with caution and only in cases where nonlinear prebuckling effects may

be neglected or at least the buckling load of the final linear buckling optimized design is verified by a GNL analysis.

6. Conclusions

General type buckling behaviour of composite structures can reliably be improved by the proposed optimization method. The method include loss of stability due to bifurcation and limiting behaviour depending on what is encountered first on the equilibrium path. A more precise estimate than classical linear buckling analysis is obtained by performing accurate nonlinear path tracing analysis and estimating the buckling load at a precritical point on the deformed structure. Features for detecting bifurcation and limit points have been developed for this purpose. General sensitivity formulas for the nonlinear buckling load, described by discretized finite element matrix equations, have been derived and the design sensitivities are approximated at the precritical point, thus no exact and troublesome determination of the exact critical point is necessary.

Shell buckling today is still a challenging task and the complicated behaviour that may be encountered can be difficult to analyze. This has been demonstrated by a thorough assessment of a classical buckling benchmark example introduced by [5]. The original solution to this immediate simple well-known example was lately proved to be incorrect by [6, 7] and is also included and treated in the book by [8]. But also their solution to the problem turns out to be incorrect. During the assessment of the shell benchmark problem in this paper it has been shown that the shell looses its stability due to bifurcation and that the bifurcation point is unstable and not stable as stated in [6, 7, 8]. In fact the bifurcation point is an unstable symmetric point of bifurcation.

The general type nonlinear buckling optimization method has been applied successfully in the buckling optimization of a composite cylindrical shell using fiber angle parametrization. Problems related to local minima and non-convexity in design space were encountered in one out of three optimization cases and caused the objective function value not to increase monotonously. It is well known that fiber angle optimization contains these issues but since the optimization method and formulas presented in this paper are generic it may easily be applied for more well behaved parametrizations.

The optimization examples demonstrated the importance of the nonlinear buckling formulation and that the type of stability should be considered since it may change during optimization. The bound formulation was applied in the studies in order to avoid problems related to mode switching if several stability points come close during optimization. Such a situation did however not occur in the general type nonlinear buckling optimization despite the type of stability changed during optimization, i.e. the same mode of stability was always optimized and depending on symmetry in design appeared as a load limit point or bifurcation point.

The general type nonlinear buckling formulation was benchmarked against the traditional linear buckling formulation and much better optimization results were obtained by the general type nonlinear buckling formulation. The linear buckling formulation did improve the buckling resistance to some extent despite poor prediction of the stability load. Linear buckling analysis is often used to predict instability and to optimize structures for maximum buckling

performance without considering nonlinear effects or type of stability. Precautions should be taken before applying the linear buckling formulation, especially in cases with nonlinear prebuckling path and in cases with limit point instability.

Using the general type nonlinear buckling optimization formulation, structures can reliably be optimized with respect to a general type stability, i.e. either bifurcation or limit point stability, and especially in cases where geometrically nonlinear effects cannot be ignored. This allows the material utilization of buckling critical laminated structures to be pushed to the limit in an efficient way yet allowing lighter and stronger structures.

Acknowledgements

[1] S. Abrate, Optimal design of laminated plates and shells, Compos. Struct. 29 (1994) 269–286.

[2] E. Riks, An incremental approach to the solution of snapping and buckling, Int. J. Solids Struct. 15 (1979) 529–551.

[3] E. Ramm, Strategies for tracing nonlinear responses near limit points, in: E. S. W. Wunderlich, K. J. Bathe (Eds.), Nonlinear finite element analysis in structural mechanics, Springer Verlag Berlin Heidelberg New York, 1981, pp. 63–89.

[4] M. A. Crisfield, A fast incremental/iterative solution procedure that handles "snap-through", Compt. Struct. 13 (1981) 55–62.

[5] A. Sabir, A. Lock, The application of finite elements to the large deflection geometrically non-linear behaviour of cylindrical shells, in: C. Brebbia, H. Tottenham (Eds.), Variational Methods in Engineering, Vol. 2, Southampton University Press, 1973, pp. 7/66–7/75.

[6] B. Wardle, The incorrect benchmark shell buckling solution, in: Collection of Technical Papers - AIAA/ASME/ASCE/AHS/ASC Structures, Structural Dynamics and Materials Conference 8, 2006, pp. 5263–5273.

[7] B. Wardle, Solution to the incorrect benchmark shell-buckling problem, AIAA J. 46 (2) (2008) 381–387.

[8] R. Jones, Buckling of bars, plates, and shells, Bull Ridge Publishing, 2006, ISBN: 0-9787223-0-2.

[9] G. Sun, J. Hansen, Optimal design of laminated-composite circular-cylindrical shells subjected to combined loads, J. Appl. Mech. 55 (1) (1988) 136–142.

[10] A. Muc, Optimal fibre orientation for simply-supported angle-ply plates under biaxial compression, Compos. Struct. 9 (1988) 161–172.

[11] G. Sun, A practical approach to optimal design of laminated cylindrical shells for buckling, Compos. Sci. Technol. 36 (1989) 243–253.

[12] S. Adali, K. J. Duffy, Design of antisymmetric hybrid laminates for maximum buckling load: I. Optimal fibre orientation, Compos. Struct. 14 (1990) 49–60.

[13] K. J. Duffy, S. Adali, Design of antisymmetric hybrid laminates for maximum buckling load: II. Optimal layer thickness, Compos. Struct. 14 (1990) 113–124.

[14] J. L. Grenestedt, Layup optimization against buckling of shear panels, Struct. Optim. 3 (1991) 115–120.

[15] H. Fukunaga, H. Sekine, M. Sato, A. Iino, Buckling design of symmetrically laminated plates using lamination parameters, Compt. Struct. 57 (1995) 643–649.

[16] M. Walker, T. Reiss, S. Adali, Multiobjective design of laminated cylindrical shells for maximum torsional and axial buckling loads, Compt. Struct. 62 (2) (1997) 237–242.

[17] C. G. Diaconu, H. Sekine, Layup optimization for buckling of laminated composite shells with restricted layer angles, AIAA J. 42 (10) (2004) 2153–2163.

[18] S. Honda, Y. Narita, K. Sasaki, Optimization for the buckling loads of laminated composite plates – comparison of various methods, Key Eng. Mater. 334-335 (2007) 89–92.

[19] C. C. Lin, A. J. Yu, Optimum weight design of composite laminated plates, Compt. Struct. 38 (5/6) (1991) 581–587.

[20] M. W. Hyer, H. H. Lee, The use of curvilinear fiber format to improve buckling resistance of composite plates with central circular holes, Compos. Struct. 18 (5/6) (1991) 239–261.

[21] M. Walker, S. Adali, V. Verijenko, Optimization of symmetric laminates for maximum buckling load including the effects of bending-twisting coupling, Compt. Struct. 58 (2) (1996) 313–319.

[22] M. Walker, Multiobjective design of laminated plates for maximum stability using the finite element method, Compos. Struct. 54 (2001) 389–393.

[23] U. Topal, Ü. Uzman, Maximization of buckling load of laminated composite plates with central circular holes using mfd method, Struct. Multidiscip. Optim. 35 (2008) 131–139.

[24] H. T. Hu, S. S. Wang, Optimization for buckling resistance of fiber-composite laminate shells with and without cutouts, Compos. Struct. 22 (2) (1992) 3–13.

[25] H. C. Mateus, C. M. M. Soares, C. A. M. Soares, Buckling sensitivity analysis and optimal design of thin laminated structures, Compt. Struct. 64 (1-4) (1997) 461–472.

[26] J. P. Foldager, J. S. Hansen, N. Olhoff, Optimization of the buckling load for composite structure taking thermal effects into account, Struct. Multidiscip. Optim. 21 (2001) 14–31.

[27] H. T. Hu, J. S. Yang, Buckling optimization of laminated cylindrical panels subjected to axial compressive load, Compos. Struct. 81 (2007) 374–385.

[28] E. Lund, Buckling topology optimization of laminated multi-material composite shell structures, Compos. Struct. 91 (2009) 158–167.

[29] U. Topal, Multiobjective optimization of laminated composite cylindrical shells for maximum frequency and buckling load, Mater. Des. 30 (2009) 2584–2594.

[30] J. S. Moita, J. I. Barbosa, C. M. M. Soares, C. A. M. Soares, Sensitivity analysis and optimal design of geometrically non-linear laminated plates and shells, Compt. Struct. 76 (2000) 407–420.

[31] E. Lindgaard, E. Lund, Nonlinear buckling optimization of composite structures, Compt. Methods Appl. Mech. Engrg. 199 (37-40) (2010) 2319–2330. doi:10.1016/j.cma.2010.02.005.

[32] E. Lindgaard, E. Lund, K. Rasmussen, Nonlinear buckling optimization of composite structures considering "worst" shape imperfections, Int. J. Solids Struct. In press. doi:10.1016/j.ijsolstr.2010.07.020.

[33] J. Thompson, The elastic instability of a complete spherical shell, Aero. Quart. 13 (1962) 189–201.

[34] J. Thompson, A general theory for the equilibrium and stability of discrete conservative systems, Z. Angew. Math. Phys. 20 (1969) 797–846.

[35] D. Bushnell, Computerized Buckling Analysis of Shells, Martinus Nijhoff Publishers, Dordrecht, The Netherlands, 1985, ISBN 90-247-3099-6.

[36] L. Johansen, E. Lund, J. Kleist, Failure optimization of geometrically linear/nonlinear laminated composite structures using a two-step hierarchical model adaptivity, Compt. Methods Appl. Mech. Engrg. 198 (30-32) (2009) 2421–2438.

[37] E. N. Dvorkin, K. J. Bathe, A continuum mechanics based four-node shell element for general non-linear analysis, Eng. Comput. 1 (1984) 77–88.

[38] M. Harnau, K. Schweizerhof, About linear and quadratic "solid-shell" elements at large deformations, Compt. Struct. 80 (9-10) (2002) 805–817.

[39] S. Klinkel, F. Gruttmann, W. Wagner, A continuum based three-dimensional shell element for laminated structures, Compt. Struct. 71 (1) (1999) 43–62.

[40] B. Brendel, E. Ramm, Linear and nonlinear stability analysis of cylindrical shells, Compt. Struct. 12 (1980) 549–558.

[41] E. Hinton (Ed.), NAFEMS Introduction to Nonlinear Finite Element Analysis, Bell and Bain Ltd, Glasgow, 1992, ISBN 1-874376-00-X.

[42] M. A. Crisfield, Non-Linear Finite Element Analysis of Solids and Structures, Vol. 1, John Wiley & Sons, Inc., 1997, ISBN 0-471-97059-X.

[43] E. L. Wilson, T. Itoh, An eigensolution strategy for large systems, Compt. Struct. 16 (1983) 259–265.

[44] A. P. Seyranian, E. Lund, N. Olhoff, Multiple eigenvalues in structural optimization problems, Struct. Optim. 8 (1994) 207–227.

[45] M. P. Bendsøe, N. Olhoff, J. Taylor, A variational formulation for multicriteria structural optimization, J. Struct. Mech. 11 (1983) 523–544.

[46] J. Taylor, M. Bendsøe, An interpretation of min-max structural design problems including a method for relaxing constraints, Int. J. Solids Struct. 20 (4) (1984) 301–314.

[47] N. Olhoff, Multicriterion structural optimization via bound formulation and mathematical programming, Struct. Optim. 1 (1989) 11–17.

[48] K. Svanberg, Method of moving asymptotes - a new method for structural optimization, Int. J. Numer. Methods Eng. 24 (1987) 359–373.

[49] MUST website, www.me.aau.dk/MUST/ (2010).

[50] ANSYS, Version 11.0, www.anys.com/ (2010).

[51] B. O. Almroth, F. A. Brogan, Bifurcation buckling as an approximation of the collapse load for general shells, AIAA J. 10 (4) (1972) 463–467.

[52] R. D. Cook, D. S. Malkus, M. E. Plesha, R. J. Witt, Concepts and Applications of Finite Element Analysis, 4th Edition, John Wiley & Sons, Inc., 2002, ISBN 0-471-35605-0.

[53] M. Tudela, P. Lagace, B. Wardle, Buckling response of transversely loaded composite shells, part 1: Experiments, AIAA J. 42 (7) (2004) 1457–1464.

[54] B. Wardle, P. Lagace, M. Tudela, Buckling response of transversely loaded composite shells, part 2: Numerical analysis, AIAA J. 42 (7) (2004) 1465–1472.